CrossMark

Synthesis and characterization of magnetic $(Cr_{0.5}Mn_{0.5})_2GaC$ thin films

Andrejs Petruhins[1] · Arni Sigurdur Ingason[1] · Jun Lu[1] · Fridrik Magnus[2] ·
Sveinn Olafsson[3] · Johanna Rosen[1]

Abstract Growth of $(Cr_{0.5}Mn_{0.5})_2GaC$ thin films from C, Ga, and compound $Cr_{0.5}Mn_{0.5}$ targets is reported for depositions on MgO (111), 4H-SiC (0001), and Al_2O_3 (0001) with and without a NbN (111) seed layer. Structural quality is found to be highly dependent on the choice of substrate with MgO (111) giving the best results as confirmed by X-ray diffraction and transmission electron microscopy. Phase pure, high crystal quality MAX phase thin films are realized, with a Cr:Mn ratio of 1:1. Vibrating sample magnetometry shows a ferromagnetic component from 30 K up to 300 K, with a measured net magnetic moment of 0.67 μ_B per metal (Cr + Mn) atom at 30 K and 5 T. The temperature dependence of the magnetic response suggests competing magnetic interactions with a resulting non-collinear magnetic ordering.

✉ Andrejs Petruhins
anpet@ifm.liu.se

Arni Sigurdur Ingason
arnsi@ifm.liu.se

Jun Lu
junlu@ifm.liu.se

Fridrik Magnus
fridrik.magnus@physics.uu.se

Sveinn Olafsson
sveinol@hi.is

Johanna Rosen
johro@ifm.liu.se

[1] Thin Film Physics, Department of Physics, Chemistry and Biology (IFM), Linköping University, 581 83 Linköping, Sweden

[2] Department of Physics and Astronomy, Uppsala University, Box 530, 751 21 Uppsala, Sweden

[3] Science Institute, University of Iceland, Dunhaga 3, 107 Reykjavik, Iceland

Introduction

MAX phases belong to a family of nanolaminated ternary compounds with the general composition $M_{n+1}AX_n$ (M–early transition metal, A–A-group element, X–C or N, $n = 1$–3). Since their discovery in the 1960s [1], it took another 30 years before they attracted an increased attention due to their unique combination of metallic and ceramic properties. To date, more than 60 MAX phases have been synthesized and characterized [2].

If one of the elements in the MAX phase is partly substituted by another on either the M, A, or X site, a solid solution can be formed. This is usually achieved by choosing substituting elements that have previously been used for MAX phase synthesis. Recently, in a quest for the first magnetic MAX phase, and fuelled by theoretical predictions [3], Mn was added as a new element to the MAX phase family. Initially, it was an alloying element in $(Cr_{1-x}Mn_x)_2AlC$ [4–7] and $(Cr_{1-x}Mn_x)_2GeC$ [8], providing the first magnetic MAX phases. Subsequent experimental studies on magnetic properties of MAX phases have not only been done on alloys containing Mn [9, 10] but the topic has also been addressed for other MAX phases like, Cr_2AlC [11], Cr_2GeC [12], and Cr_2GaN [13]. Recently, a new MAX phase with Mn as the sole M element, Mn_2GaC, was theoretically predicted [14] and experimentally confirmed [15], and it was also shown to have magnetic ordering.

Moreover, $(Cr_{1-x}Mn_x)_2GaC$ solid solutions have been synthesized in bulk form, for $x = 0.3$ showing magnetic transition temperatures at 38 and 153 K [5], and for

nominally $x = 0.5$ showing indications of ferrimagnetism [16]. However, in the latter study, x denoted the initial Cr/Mn precursor ratio, and not a demonstrated Mn incorporation in the MAX phase structure. A more recent study has shown that precursor ratios cannot be unambiguously used to determine the composition of the final structure, and for both $(Cr_{1-x}Mn_x)_2AlC$ and $(Cr_{1-x}Mn_x)_2GaC$ the Mn solubility limit seems to be lower in bulk than in corresponding thin films [5].

No alloy thin films of $(Cr_{1-x}Mn_x)_2GaC$ ($0 < x < 1$) have hitherto been reported. Such films, with high structural quality and a well-defined composition, could be used to investigate the effects of Mn alloying in the Cr_2GaC phase, in line with previous work [4, 7, 8]. This is crucial to ensure that measured thin film properties are an effect of Mn alloying and do not originate from competing magnetic phases or compositional deviations from assumed alloy stoichiometry. The objective of this study is to investigate the effect of Mn alloying in Cr_2GaC films, in particular their magnetic properties, as prior investigations on this material in bulk form indicate magnetic characteristics. We have therefore grown $(Cr_{1-x}Mn_x)_2GaC$ ($x = 0.50$) thin films of high purity and high structural quality, and investigated in detail their structure, composition, and magnetic properties.

Experimental details

Films were deposited by magnetron sputter epitaxy using three elemental targets: Carbon (99.99 % purity), compound Cr/Mn with 50:50 at.% (99.95 % purity) and gallium (99.9999 % purity). The base pressure in the deposition chamber was below 5×10^{-9} Torr, and the Ar pressure was 4.5 m Torr. For Mn and C, three inch targets were used, confocally placed at a $35°$ angle with respect to the substrate normal at a distance of 180 mm. For Ga, a two inch sputtering target was prepared according to details described elsewhere [17], and placed directly below the substrate (on axis) at a distance of 180 mm.

Sputtering targets were operated in constant current mode and were set to calibrated room temperature fluxes corresponding to 2:1:1 for Cr/Mn, Ga and C, respectively. The applied current process set points were then fine-tuned to optimize the resulting film composition at the synthesis temperature.

To investigate growth on different substrates with various lattice mismatches with respect to the MAX phase, films were grown on Al_2O_3 (0001), MgO (111), 4H-SiC (0001) with $4°$ off–cut toward the $[11\bar{2}0]$ direction as well as Al_2O_3 (0001) with a deposited ~ 15 nm thick NbN (111) seed layer, which prior to deposition were cleaned in ultrasonic baths of acetone, ethanol, and isopropanol for

10 min, and then were kept at the deposition temperature of 600 °C for 60 min prior to deposition to ensure uniform temperature distribution.

The structural properties of the films were investigated through X-ray diffraction (XRD) and X-ray reflectivity (XRR), using standard θ–2θ geometry, and pole figure measurements in a Panalytical Empyrean MRD with Cu Kα radiation ($\lambda = 1.54$ Å). The scans were obtained with the tube in line focus using a Ge (220) hybrid monochromator on the incident side and a $0.27°$ collimator on the diffracted side, with or without a collimator slit depending on the measurement. To evaluate sample quality, high resolution rocking curves were performed using a channel cut Ge (220) analyzer on the diffracted side. The reflectivity data were fitted using the Panalytical X'pert Reflectivity software.

The sample was prepared for cross-sectional (scanning) transmission electron microscopy, (S)TEM by conventional mechanical polishing and Ar-ion milling methods. TEM was performed using a Tecnai G2 TF20 UT electron microscope, operated at 200 kV. Images were acquired in TEM mode using a CCD camera. Energy dispersive X-ray spectroscopy (EDX) was performed in STEM mode. STEM imaging and EDX-mapping was performed on the doubly corrected Linköping Titan³ 60–300. The STEM images were recorded by the high-angle annular dark-field (HAADF) detector. The same electron probe was used for the STEM-EDX mapping, employing Super-X detectors.

The magnetic response of the sample was measured in a vibrating sample magnetometer (VSM) in the temperature range 30–300 K with the magnetic field applied parallel to the film plane. All temperature changes were done with no magnetic field applied. The sample was first cooled down to the lower temperature followed by magnetization measurement at different fields and afterward heating up to next measurement temperature. The magnetic response of the MgO substrate was measured separately, as a function of temperature, and subtracted from the total substrate-film signal. It should be noted that measurements were performed also below 30 K but in this temperature range the non-linear MgO background could not be unambiguously separated from the signal originating from the MAX phase. Hence, the low-temperature analysis is beyond the scope of the present work.

Results and discussion

Structural characterization

X-ray diffraction analysis of a thin film grown on a MgO (111) substrate for 10 min is shown in Fig. 1. Apart from MgO 111 and 222 peaks, only basal plane MAX phase
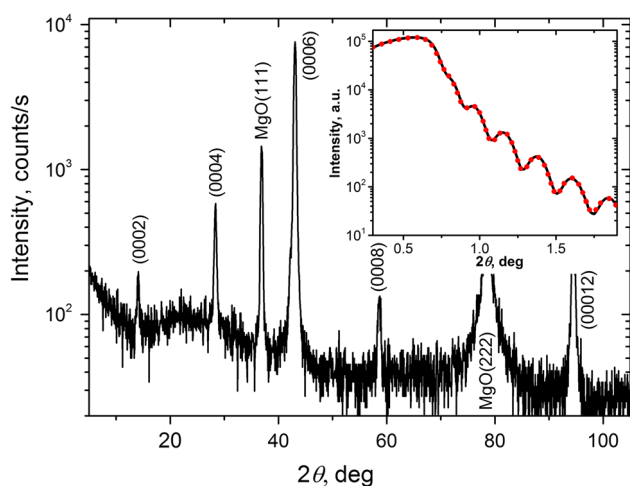
Fig. 1 XRD θ–2θ scan of a $(Cr_{1-x}Mn_x)_2GaC$ thin film grown on MgO (111). The inset shows XRR measurement data (*dots*), along with a fitted curve (*line*)

peaks can be seen, with no traces of other crystalline phases. The expected epitaxial relationship between film and substrate is $[11\bar{2}0]_{MAX}\|[10\bar{1}]_{MgO}$ in the film plane and $[0001]_{MAX}\|[111]_{MgO}$ out of the plane. The inset of Fig. 1 shows XRR data (dots) fitted with a single layer model (line), which gives a film thickness of 33.5 ± 0.6 nm. The estimated roughness and density of the film is 1.7 ± 0.6 nm and 6.4 ± 0.4 g/cm^3, respectively. Measurements of the asymmetric $(10\bar{1}3)$ and in-plane $(11\bar{2}0)$ plane spacing gave the lattice parameter $a = 2.897 \pm 0.001$ Å, whereas $c = 12.596 \pm 0.002$ Å was determined from (0006) plane spacing. These lattice parameters yield a unit cell volume of 91.55 ± 0.08 Å^3. Comparing these values to pure Cr_2GaC [17] ($a = 2.90$ Å and $c = 12.62$ Å) and Mn_2GaC [15] ($a = 2.90$ Å and $c = 12.57$ Å) for thin films on the same type of substrate and of similar thickness, the in-plane lattice parameter does not change significantly over the full range of Cr/Mn ratios, while the c lattice parameter lies approximately in the middle between values of Cr_2GaC and Mn_2GaC, consistent with what one might expect from Vegard's law [18] for a composition of $(Cr_{0.5}Mn_{0.5})_2GaC$.

A series of samples with different thickness were also grown on MgO (111) substrates. The thickness of a 34 nm and a 95 nm sample was determined from XRR, whereas samples of ~ 190 and ~ 570 nm were approximated from the calculated growth rate of the samples measured by XRR. Evolution of lattice parameters with a changed film thickness was evaluated by XRD, showing no change in the in-plane lattice parameter a. The c lattice parameter, however, decreases slightly with increasing film thickness, from

12.596 ± 0.002 Å for the 34 nm film to 12.584 ± 0.002 Å for the ~ 570 nm film, which could indicate film relaxation.

Figure 2a shows the low magnification TEM image of the film (middle) and substrate (bottom). The top layer is the glue remaining from the sample preparation process. The film consists of uniform high quality epitaxial MAX phase of ~ 33 nm thickness, consistent with the XRR analysis. A grain size above at least 150 nm allows identification of uninterrupted MAX phase basal planes throughout the film section presented in (a). Figure 2b shows higher resolution epitaxial MAX phase throughout the whole film thickness. A HAADF image is shown in Fig. 2c and the same area is mapped with EDX. Elemental maps in Fig. 2d, e, and f, show a uniform elemental distribution of the Cr, Mn, and Ga content in the MAX phase structure, also evident from the EDX spectrum in (g), which yields an atomic ratio of approximately 35:34:31 for Cr, Mn, and Ga, respectively. Apart from the aforementioned elements, C and Ti can also be seen, where C is a constituent of the MAX phase and Ti is residue from the sample preparation process (the sample is mounted in a Ti grid).

XRD analysis of a sample grown on a Al_2O_3 (0001) substrate is shown in Fig. 3. The basal plane MAX phase and Al_2O_3 (000ℓ) substrate peaks can be seen, as well as asymmetric $(10\bar{1}3)$ and $(10\bar{1}0)$ peaks from the MAX phase, indicating growth of secondary oriented grains. Similar tilted grain growth on Al_2O_3 (0001) substrates has been previously observed for Cr_2GeC thin films [19]. Tilting the sample to measure the asymmetric peak $(10\bar{1}3)$, allows indirect determination of the lattice parameters to $a = 2.904 \pm 0.001$ Å and $c = 12.582 \pm 0.002$ Å, resulting in a unit cell volume of 91.89 ± 0.08 Å^3.

An XRD scan of a sample grown on 4° off-cut 4H-SiC (0001) for 30 min is shown in Fig. 4. MAX phase basal plane and substrate peaks, as well as peaks from tilted $(10\bar{1}3)$ MAX phase grains are visible. The presence of $(10\bar{1}3)$ grains is confirmed by doing off-axis XRD measurements (not shown) at $\chi = 59.4°$ (the angle between (0006) and $(10\bar{1}3)$ planes), where the presence of (0006) spacing is evident. There are, however, minor peaks at 2θ $\sim 31.9°$ and $\sim 45.9°$ originating most likely from the Mn_3GaC inverse perovskite, marked as dots in Fig. 4. These peaks are minute in comparison to MAX phase peaks, as the diffractogram shown in Fig. 4 is displayed in logarithmic scale on the intensity axis and these impurity phase peaks are almost three orders of magnitude lower in intensity than the most intense basal plane peak of the MAX phase. The θ offset was specified by the (0006) peak of the MAX phase, thus the peaks at $\sim 35.5°$ and $\sim 75.5°$ originate from the 4H-SiC substrate, though of significantly reduced intensity. The expected epitaxial relationship

Fig. 2 TEM analysis of a $(Cr_{0.5}Mn_{0.5})_2GaC$ thin film grown for 10 min. a Low magnification micrograph of the film (*middle*) and substrate (*bottom*) with remains of the glue from the sample preparation process (*top*). b High magnification micrograph revealing epitaxial MAX phase layers throughout the film thickness. c HAADF image of the region where EDX mapping was performed using Ga–L (d), Cr–K (e), and Mn–K (f) edges. g EDX spectrum obtained from the MAX phase region
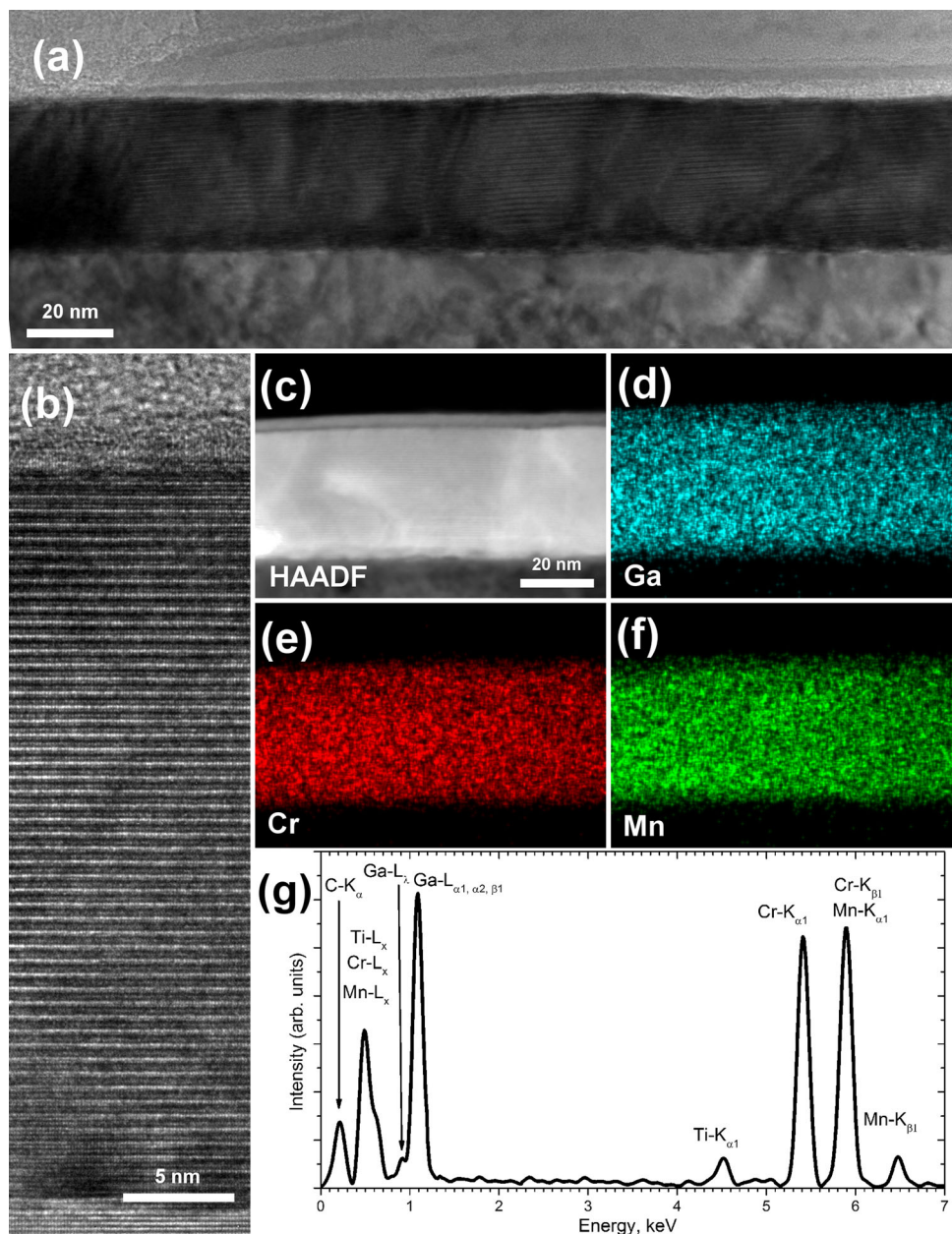
between film and substrate is $[11\overline{2}0]_{MAX}\|[11\overline{2}0]_{4H-SiC}$ in the film plane and $[0001]_{MAX}\|[0001]_{4H-SiC}$ out of the plane. The lattice parameters determined from the XRD measurements give values of $a = 2.911 \pm 0.001$ Å and $c = 12.549 \pm 0.002$ Å, and a unit cell volume of 92.09 ± 0.08 Å^3. This is a slight increase in a accompanied by a decrease in c, however, with an increase of the unit cell volume compared to corresponding films grown on both MgO (111) and Al_2O_3 (0001).

A sample was grown for 3 h on Al_2O_3 (0001) with a high quality ~ 15 nm thick NbN (111) seed layer, to reduce the lattice mismatch and facilitate MAX phase growth. This resulted in a highly textured film, as

confirmed by XRD analysis, see Fig. 5. Apart from very high intensity basal plane peaks, a relatively minor quantity of $(10\overline{1}3)$ grains are present, as the $(10\overline{1}3)$ peak intensity is about two orders of magnitude lower than the intensity originating from (0006). Pole figure measurements show that apart from the major epitaxial orientation of the film, there are four other, minor, epitaxial directions for the MAX phase crystal (see Fig. 5 inset). These directions correspond to the MAX phase grains that are rotated $\pm 12°$ and $\pm 24°$ with respect to the majority of MAX phase grains. The intensity as measured by XRD of these grains is approximately one and two orders of magnitude lower for $\pm 12°$ and $\pm 24°$ rotated grains, as compared to the majority
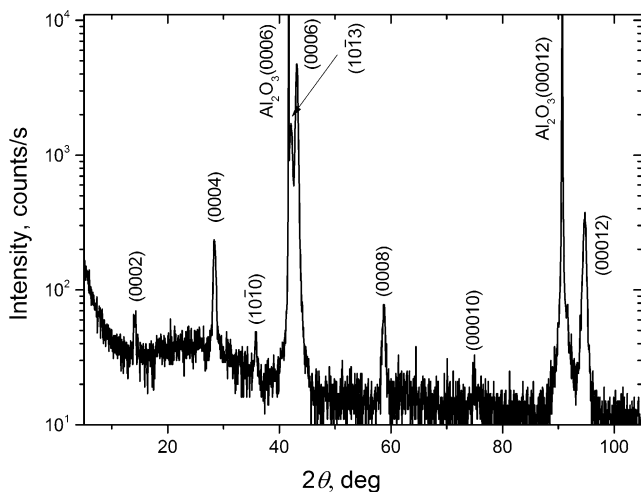
Fig. 3 XRD θ–2θ scan of $\sim$34 nm thick $(Cr_{1-x}Mn_x)_2GaC$ sample grown on Al_2O_3 (0001)
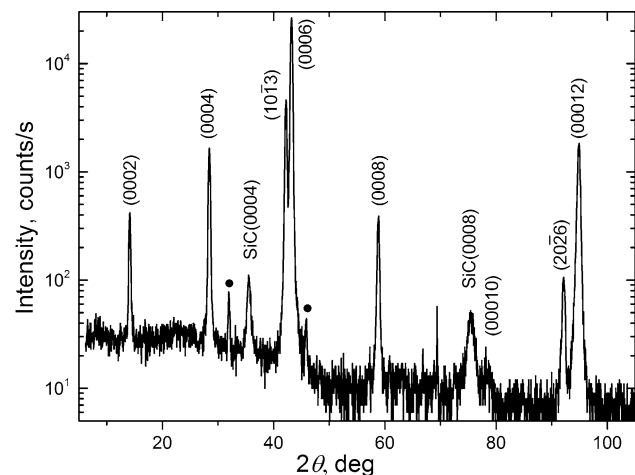
Fig. 4 XRD θ–2θ scan of a $\sim$95 nm thick $(Cr_{1-x}Mn_x)_2GaC$ sample grown on 4° off-cut 4H-SiC (0001). *Black dots* indicate the peaks corresponding to Mn_3GaC inverse perovskite impurity phase

Fig. 5 XRD θ–2θ scan of a $\sim$570 nm thick $(Cr_{1-x}Mn_x)_2GaC$ sample grown on Al_2O_3 (0001) with NbN (111) seed layer. The inset shows a pole figure of the $(10\bar{1}3)$ MAX phase peak ($2\theta = 41.8°$)

Table 1 Summary of substrate in-plane lattice spacings matching MAX phase as well as lattice parameters and unit cell volumes of respective MAX phase grown on these substrates

Substrate	MgO	Al_2O_3	NbN	4H-SiC
In-plane lattice parameter (Å)	2.981	2.868	3.083	3.084
MAX				
a (Å)	2.897	2.904	2.908	2.911
c (Å)	12.595	12.581	12.552	12.552
Unit cell vol. (Å^3)	91.55	91.89	91.92	92.09

direction. Obtained lattice parameters for this film are $a = 2.908 \pm 0.001$ Å and $c = 12.552 \pm 0.002$ Å, and resulting unit cell volume is 91.92 ± 0.08 Å^3.

Based on the analysis presented above of films deposited on different substrates, we can conclude that the MgO (111) substrate gives the best epitaxial films in terms of high structural quality with no indications of tilted grains. The Al_2O_3 (0001) substrate with or without NbN seed layer results in a high crystal quality film, as indicated by rocking curve measurements (full width at half maximum (FWHM) of the (0006) of the MAX phase of 0.011° for the film grown on Al_2O_3 substrate without seed layer), however, an appreciable amount of secondary $(10\bar{1}3)$ oriented MAX phase grains are present, indicating that even at optimal deposition conditions, the growth of only (000ℓ)
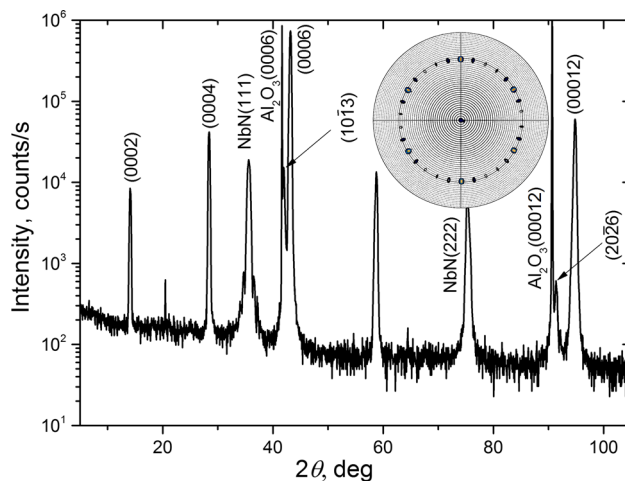
oriented MAX phase is most likely not possible. Growth of $(Cr_{1-x}Mn_x)_2GaC$ on a 4° off-cut 4H-SiC substrate results in the presence of both secondary $(10\bar{1}3)$ oriented MAX phase and other impurity phases, which indicates that this substrate requires different deposition conditions compared to those optimal for MgO (111). Rocking curve measurements performed on these samples showed that only films grown on Al_2O_3 substrate have a very narrow peaks, whereas films on other substrates showed much broader peaks with FWHM even up to of 2° on MgO (111), which could indicate at some MgO substrates were of poor quality [20]. Pole measurements of all of the presented films were performed on the $(10\bar{1}3)$ peak of the MAX phase. In pole figures (not shown) of all of the films, distinct peaks are seen at an angle of $\sim$59°, corresponding to the angle between (000ℓ) and $(10\bar{1}3)$, indicating that the films are epitaxial.

The in-plane spacings of Al_2O_3 (0001), MgO, 4H-SiC, and NbN, to which the film is adjusting its lattice parameter, is 2.868, 2.981, 3.084, and 3.083 Å, respectively, see Table 1. Comparing these values to the in-plane lattice parameter of the MAX phase (e.g., 2.897 Å as grown on

MgO (111) substrate), one would expect that Al_2O_3 (0001) is the only substrate for which the MAX phase thin films experience compressive stress, whereas the other substrates induce tensile stress. Comparing that to the actual MAX phase lattice parameter evolution on different substrates, we see that compared to films grown on MgO (111), MAX phase grown on Al_2O_3 (0001), 4H-SiC (0001) and on a NbN seed layer on top of Al_2O_3 (0001) seem to have a slightly larger in-plane lattice parameter a, followed by a decrease in lattice parameter c, as expected. It is not, however, clear, why an expansion in-plane is present for films grown on Al_2O_3 (0001), as the adapting in-plane lattice spacing is smaller than that of MgO (111). This is possibly because on the surface of the Al_2O_3 (0001) crystal, there is more complex nucleation of the MAX phase that may not be primarily governed by the hexagonal nucleation site with the spacing of 2.868 Å.

From all substrates used, only the MgO provides the possibility for growth of single phase, single orientation $(Cr_{1-x}Mn_x)_2GaC$ thin films, as films grown on other substrates contained secondary orientation $(10\bar{1}3)$ MAX phase grains.

Magnetic properties

The in-plane magnetic response of the sample deposited on MgO was measured by VSM in the temperature range from 30 to 300 K. Figure 6 shows the isothermal magnetization curves. The films show a ferromagnetic response with small hysteresis at low applied fields (<0.2 T), see inset. However, with increasing magnetic field the magnetization
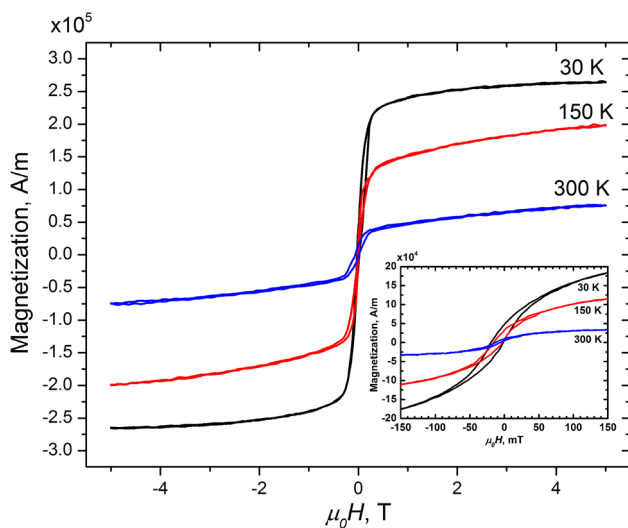
continues to rise and does not reach saturation even at 5 T for temperatures at and above 50 K. The temperature dependence of the magnetization, expressed in net magnetic moment per M atom (Cr + Mn) at 5 T, m_{5T}, and the remanent magnetization, expressed in net remanent moment per M atom, are shown in Fig. 7. Both decrease gradually with increasing temperature and no clear magnetic transition can be seen. The magnetic transition temperature is clearly above room temperature (300 K), for which m_{5T} is calculated to be 0.19 μ_B per M atom, the remanent moment is 0.004 μ_B per M atom, and the coercive field 8 mT. The m_{5T} measured at 30 K is calculated to be 0.67 μ_B per M atom, and this value appears to be the saturation magnetization. At 30 K, remanent moment is 0.036 μ_B and coercive field is 12 mT. It is worth pointing out that the saturation seems to be reached also at 50 K with similar m_{5T} value within the experimental error margins. This magnetic moment per M atom is the largest reported among Mn containing MAX phase alloy systems to date [7, 8, 15].

The unconventional temperature dependence of the remanent and 5 T magnetization, without a clear magnetic transition temperature, as well as the large saturation field, indicates that we do not have a simple collinear ferromagnetic ordering. A large saturation field alone could point toward a large magneto crystalline anisotropy, but studies on a neighboring Mn-based magnetic MAX phase $(Cr_{1-x}Mn_x)_2GeC$ have not shown the basal plane to have a magnetically hard axis [8]. Furthermore, the magnetization does not follow the $(T_c - T)^\beta$ temperature dependence characteristic of ferromagnets. Instead, the results suggest a non-collinear magnetic state with a small ferromagnetic component, which increases with decreasing temperature. Such an arrangement can be a result of competing magnetic
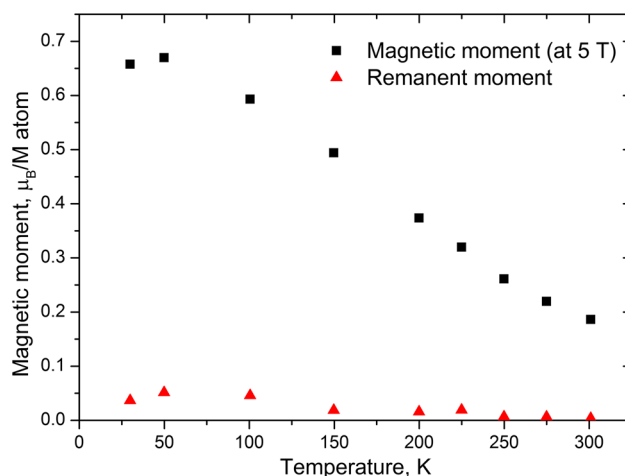
Fig. 6 In-plane magnetization versus magnetic field measured at 30, 150, and 300 K, showing an S-shape magnetic response at all temperatures. The *inset* expands the low-field region, showing a clear remanent magnetization

Fig. 7 Average calculated net magnetic moment at 5 T and the average net remanent moment, expressed in μ_B per M atom in the MAX phase, versus temperature

interactions in the system, where ferromagnetic and anti-ferromagnetic states are nearly degenerate, as has been suggested for the neighboring $(Cr_{1-x}Mn_x)_2GeC$ and closely related Mn_2GaC [8, 15]. This delicate balance between different magnetic configurations leads to a complex temperature dependence, where the ferromagnetic state can be of lower energy at low temperatures.

The magnetic behavior presented here is different from what has been previously reported for bulk $(Cr_{1-x}Mn_x)_2GaC$. In one study [16], for an assumed composition of $x = 0.5$, a paramagnetic behavior with weak ferrimagnetism was suggested as the ground state based on measurements at 5 K. The reported temperature dependence of the magnetism, however, showed an approximately linear trend in the temperature range of 30–300 K, and no remanence or coercivity was reported for any isothermal measurement. In another study on bulk MAX phase synthesis [5], it was shown that using initial precursor molar ratios of 1:1 for Cr and Mn, the final MAX phase composition included less Mn, giving a nominal composition of $(Cr_{0.7}Mn_{0.3})_2$ GaC. This material showed two magnetic transitions—at 38 K and at 153 K, which did not correspond to any transition temperature of previously known magnetic phases in the Cr–Mn–Ga–C system, or any of the observed impurity phases concluded from phase analysis. Hence, $(Cr_{0.7}Mn_{0.3})_2$ GaC was suggested to be magnetic. Comparing these results to those of the present paper, it is clear that the magnetic properties are strongly dependent on the Mn content.

Conclusions

We have demonstrated growth of epitaxial $(Cr_{0.5}Mn_{0.5})_2GaC$ thin films on MgO (111), Al_2O_3 (0001), and 4° off-cut 4H-SiC (0001) substrates. Deposited films are smooth and exhibit X-ray reflectivity interference fringes for thicknesses of up to $\sim$100 nm. TEM analysis confirms a high crystal quality and a local composition corresponding to $(Cr_{0.5}Mn_{0.5})_2GaC$. Films grown on Al_2O_3 (0001) are phase pure, however, tilted grain growth is evident, thus more optimal MAX phase growth is found on MgO (111) substrates.

Magnetic measurements on the film deposited on MgO reveal a ferromagnetic response from 30 K up to room temperature, with the net magnetization at 5 T decreasing gradually with increasing temperature. The magnetic moment measured at 5 T and 30 K is 0.67 μ_B per M atom. The temperature dependence of the remanent and 5 T magnetization, as well as a large saturation field, suggest competing magnetic interactions in the system and non-collinear magnetic ordering.

References

1. Nowotny VH (1971) Strukturchemie einiger Verbindungen der Übergangsmetalle mit den elementen C, Si, Ge, Sn. Prog Solid State Chem 5:27–70
2. Barsoum MW (2013) MAX phases: properties of machinable ternary carbides and nitrides. Wiley, Boston
3. Dahlqvist M, Alling B, Abrikosov IA, Rosen J (2011) Magnetic nanoscale laminates with tunable exchange coupling from first principles. Phys Rev B 84(22):220403
4. Mockute A, Dahlqvist M, Emmerlich J, Hultman L, Schneider JM, Persson POÅ, Rosen J (2013) Synthesis and ab initio calculations of nanolaminated (Cr, Mn) 2 AlC compounds. Phys Rev B 87(9):094113
5. Mockute A, Lu J, Moon EJ, Yan M, Anasori B, May SJ, Barsoum MW, Rosen J (2014) Solid solubility and magnetism upon Mn incorporation in the bulk ternary carbides Cr_2AlC and Cr_2GaC. Mater Res Lett 3(1):16–22
6. Mockute A, Persson POÅ, Lu J, Ingason AS, Magnus F, Olafsson S, Hultman L, Rosen J (2014) Structural and magnetic properties of $(Cr_{1-x} Mn_x)5Al8$ solid solution and structural relation to hexagonal nanolaminates. J Mater Sci 49(20):7099–7104
7. Mockute A, Persson POÅ, Magnus F, Ingason AS, Olafsson S, Hultman L, Rosen J (2014) Synthesis and characterization of arc deposited magnetic (Cr, Mn)2AlC MAX phase films. Phys Status Solidi Rapid Res Lett 8(5):420–423
8. Ingason AS, Mockute A, Dahlqvist M, Magnus F, Olafsson S, Arnalds UB, Alling B, Abrikosov IA, Hjörvarsson B, Persson POÅ, Rosen J (2013) Magnetic self-organized atomic laminate from first principles and thin film synthesis. Phys Rev Lett 110(19):195502
9. Tao QZ, Hu CF, Lin S, Zhang HB, Li FZ, Qu D, Wu ML, Sun YP, Sakka Y, Barsoum MW (2014) Coexistence of ferromagnetic and a re-entrant cluster glass state in the layered quaternary $(Cr_{1-x}, Mn_x)2GeC$. Mater Res Lett 2(4):1–7
10. Liu Z, Waki T, Tabata Y, Nakamura H (2014) Mn-doping-induced itinerant-electron ferromagnetism in Cr_2GeC. Phys Rev B 89(5):054435
11. Jaouen M, Chartier P, Cabioc'h T, Mauchamp V, André G, Viret M (2013) Invar like behavior of the Cr_2AlC MAX phase at low temperature. J Am Ceram Soc 96(12):3872–3876
12. Jaouen M, Bugnet M, Jaouen N, Ohresser P, Mauchamp V, Cabioc'h T, Rogalev A (2014) Experimental evidence of Cr magnetic moments at low temperature in Cr_2A (A = Al, Ge) C. J Phys Condens Mat 26(17):176002
13. Liu Z, Waki T, Tabata Y, Yuge K, Nakamura H, Watanabe I (2013) Magnetic ground state of the M_{n+1} n-phase nitride Cr_2GaN. Phys Rev B 88(13):134401
14. Thore A, Dahlqvist M, Alling B, Rosén J (2014) First-principles calculations of the electronic, vibrational, and elastic properties of the magnetic laminate Mn_2GaC. J Appl Phys 116(10):103511
15. Ingason AS, Petruhins A, Dahlqvist M, Magnus F, Mockute A, Alling B, Hultman L, Abrikosov IA, Persson POÅ, Rosen J

(2013) A nanolaminated magnetic phase: Mn$_2$GaC. Mater Res Lett 2(2):89–93

16. Lin S, Tong P, Wang BS, Huang YN, Lu WJ, Shao DF, Zhao BC, Song WH, Sun YP (2013) Magnetic and electrical/thermal transport properties of Mn-doped Mn+1AX$_n$ phase compounds Cr$_{2-x}$Mn$_x$GaC ($0 \leq x \leq 1$). J Appl Phys 113(5):053502

17. Petruhins A, Ingason AS, Dahlqvist M, Mockute A, Junaid M, Birch J, Lu J, Hultman L, Persson POÅ, Rosen J (2013) Phase stability of Cr$_{n+1}$GaC$_n$ MAX phases from first principles and Cr$_2$GaC thin-film synthesis using magnetron sputtering from elemental targets. Phys Status Solidi Rapid Res Lett 7(11):971–974

18. Vegard L (1921) Die Konstitution der Mischkristalle und die Raumfüllung der Atome. Z Physik 5(1):17–26

19. Eklund P, Bugnet M, Mauchamp V, Dubois S, Tromas C, Jensen J, Piraux L, Gence L, Jaouen M, Cabioc'h T (2011) Epitaxial growth and electrical transport properties of Cr$_2$GeC thin films. Phys Rev B 84(7):075424

20. Schroeder JL, Ingason AS, Rosén J, Birch J Beware of poor-quality MgO substrates: A study of MgO substrate quality and its effect on thin film quality. J Cryst Growth. doi:10.1016/j.jcrysgro.2015.03.010